Journal of Catalysis 276 (2010) 114–122

Contents lists available at ScienceDirect

Journal of Catalysis

journal homepage: www.elsevier.com/locate/jcat

Kinetic characterization of unsupported ReS_2 as hydroprocessing catalyst

T.C. Ho *, Q. Shen [1], J.M. McConnachie, C.E. Kliewer

Corporate Strategic Research Labs, ExxonMobil Research and Engineering Co., Annandale, NJ 08801, United States

ARTICLE INFO

Article history:
Received 8 July 2010
Revised 2 September 2010
Accepted 4 September 2010
Available online 16 October 2010

Keywords:
Hydrodesulfurization
Hydrodenitrogenation
Rhenium sulfide
Catalyst inhibition
Diethyldibenzothiophenes
Ethylcarbazole
Competitive adsorption

ABSTRACT

The hydrodesulfurization (HDS) and hydrodenitrogenation (HDN) activities of an unsupported rhenium sulfide and a sulfided $CoMo/Al_2O_3–SiO_2$ catalyst are compared using 4,6-diethyldibenzothiophene (46DEDBT) and 3-ethylcarbazole (3ECBZ) as probe molecules. The active site densities and adsorption-reaction rate constants are determined from transient experiments. It is found that ReS_2 has an unusually high selectivity toward hydrogenation. As such, it has a far higher activity than $CoMo/Al_2O_3–SiO_2$ for desulfurizing 46DEDBT in the absence of 3ECBZ. The higher activity of ReS_2 arises from a higher turnover frequency as the active site density on ReS_2 is about one-third that on $CoMo/Al_2O_3–SiO_2$. Due to ReS_2's higher hydrogenation power, the HDS of 46DEDBT on ReS_2 is less resilient to 3ECBZ inhibition than that on $CoMo/Al_2O_3–SiO_2$. ReS_2 shows about a sevenfold activity advantage over the $CoMo/Al_2O_3–SiO_2$ catalyst in the hydrodenitrogenation of 3ECBZ. The results shed some light on the HDS–HDN interactions in real-feed deep HDS.

1. Introduction

Catalytic hydrodesulfurization (HDS) and hydrodenitrogenation (HDN) are used in the refining industry for removing indigenous organosulfur and organonitrogen species from various petroleum fractions such as middle distillates (200–370 °C boiling range; diesel, jet fuel, heating oil, etc.). The majority of the catalysts used are Al_2O_3-supported MoS_2 and/or WS_2 into which Co and Ni are incorporated as promoters [1]. The mounting concerns over the environment and the growing need to process heavier/dirtier crude oils have made it mandatory to develop new HDS and HDN catalysts for producing high-quality, ultra-clean fuels. For the HDS of a diesel molecule such as dibenzothiophene (DBT), the reaction proceeds along two pathways [1]. The hydrogenolysis pathway gives biphenyl-type products (BP) through direct sulfur extraction. The hydrogenation pathway produces cyclohexylbenzene-type products (CHB) via hydrogenation of one of the phenyl rings followed by C–S bond cleavage. More than ten years ago, diesel sulfur specifications were between 350 and 500 wppm in many countries. Refiners could meet such specifications by desulfurizing DBT and some of its alkyl derivatives. However, today's 10–15 wppm specifications in a growing number of countries require desulfurization of 4-alkyl- and 4,6-alkyl-DBTs. Desulfurization of such sterically hindered DBTs relies heavily on the hydrogenation pathway [2]. This, coupled with the dwindling supply of high-quality crude oils and the growing need to reduce organonitrogen and polynuclear aromatic species, points to the importance of catalyst's hydrogenation function. Much effort has been made to increase hydroprocessing activity via enhancement of catalyst's hydrogenation function.

Unsupported sulfides in general are known to be more selective toward hydrogenation than commercial $CoMo/Al_2O_3$ sulfide catalysts [3–5]. For instance, Hermann et al. [3] reported that unsupported sulfides of Mo, Ru, Nb, Rh, and Pd are more hydrogenation selective than sulfided $CoMo/Al_2O_3$ catalysts in the HDS of 4,6-dimethyldibenzothiophene. Unsupported RuS_2 shows a remarkably high activity for deep HDS of a tough-to-desulfurize petroleum fraction at low hydrogen pressures [6]. An unsupported metal sulfide called Nebula was recently commercialized for deep HDS and HDN applications [7]. For exploration and development of new unsupported sulfide catalysts, it is essential to gain a quantitative understanding of the differences between unsupported sulfides and conventional Al_2O_3-supported catalysts in terms of active site density and adsorptivity. Being in a poorly crystalline and highly disordered state, transition metal sulfides are notoriously difficult to characterize. The most direct way of estimating active site density is to conduct combined modeling and experimental studies under transient conditions.

MoS_2 and WS_2 are both trigonal prismatic and have a layered structure. The active sites are commonly believed to be sulfur vacancies associated with exposed Mo or W cations and SH^-/S^{2-} groups on the MoS_2/WS_2 edge [1]. Recently, nonvacancy sites have also been identified; they are metallic brim sites with remarkable

* Corresponding author.
E-mail address: teh.c.ho@exxonmobil.com (T.C. Ho).
[1] Present address: Department of Chemical Engineering, University of Texas, Austin, TX 78712, United States.

0021-9517/$ - see front matter © 2010 Elsevier Inc. All rights reserved.
doi:10.1016/j.jcat.2010.09.005

Nomenclature

g	$k_n N_f/k_{HDN}$, defined in Eq. (11)
$\bar{g}$	$k_n N_f/k'_n$
k_{HDS}	surface HDS rate constant (1/s)
k_{HDN}	surface HDN rate constant (1/s)
k_n	adsorption rate constant for nitrogen (cc feed/s/μmole)
k_o	equivalent pseudo-first-order rate constant, defined in Eq. (19).
k_s	adsorption rate constant for sulfur (cc feed/s/μmole)
k'_n	desorption rate constant for nitrogen (1/s)
k'_s	desorption rate constant for sulfur (1/s)
p	adsorption selectivity defined in Eq. (13)
N	concentration of nitrogen atom in the fluid phase (μmole/cc feed or g/cc)
N_f	feed nitrogen atom concentration, g N atom/cc or μmole/cc
q_m	catalyst maximum site capacity, μmole N adatom/g cat
q_n	concentration of adsorbed nitrogen atom on catalyst
S	concentration of sulfur atom in the fluid phase (μmole/cc feed or g/cc)
S_f	sulfur atom concentration in feed liquid, g S/cc or μmole/cc feed
$\widehat{S}$	sulfur concentration in the fluid phase at Steady State I
t	time
v	superficial velocity
z	axial distance from the entrance of the reactor (cm)

Greek symbols

ε	bed void fraction (0.3)
ρ_p	sulfided catalyst packing density in the bed (1.15 g/cc)
τ	space time based on catalyst weight
θ_n	q_n/q_m, the fractional coverage of adsorbed nitrogen

hydrogenation functionality [8]. Reduction of molybdenum in MoS_2 from Mo(IV) to Mo(III) transforms the molybdenum coordination from hexagonal to distorted octahedral, with concomitant formation of localized Mo–Mo bonds. The fully reduced compound, $LiMoS_2$, has a structure similar to ReS_2, which might be expected as Re(IV) is isoelectronic with Mo(III) [9]. Rhenium in ReS_2 is bound by sulfur in an octahedral environment, and the rhenium atoms connect through a diamond-chain motif of Re–Re bonds [10,11] as shown in Fig. 1. Rhenium sulfide and molybdenum/tungsten sulfides also share a common anisotropic characteristic, in that only a small fraction of the total surface area is expected to be catalytically active. By contrast, the isotropic structure of RuS_2 crystallites gives a high exposure of active surface metal atoms to adsorbates.

Rhenium sulfide is active for desulfurizing thiophene and DBT [12]. Jacobson et al.'s study using an indole-DBT-naphthalene mixture has indicated that the HDN activities of five unsupported metal sulfides decrease in the following order: $ReS_2 > MoS_2 > RuS_2 > NbS_2 \approx Co_9S_8$ [13]. This activity ranking was rationalized in terms of a bond energy model in which the metal–sulfur bond strengths are measured by temperature-programmed reduction of H_2S-pretreated catalysts. Jacobson et al. also reported the following HDS activity ranking: $RuS_2 > ReS_2 > MoS_2 > NbS_2 \approx Co_9S_8$. Thus, ReS_2 is an active and selective HDN catalyst based on experiments with the indole-DBT-naphthalene mixture. It is also more active than MoS_2 for both HDS and HDN. The performance difference between ReS_2 and MoS_2 may be related to their reducibility [14]. It is unclear that the high activity of unsupported rhenium sulfide is due to the number or the quality of active sites. Also, the performance of rhenium sulfide under ultra-deep HDS conditions has not been examined.

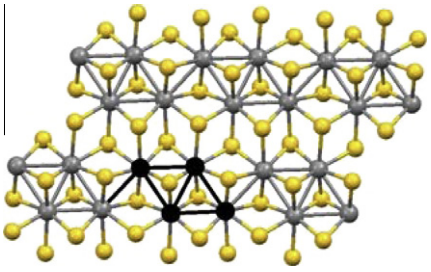

Fig. 1. Structure of ReS_2: gray ball, rhenium; yellow ball, sulfur. The metal–metal bonding is highlighted in black.

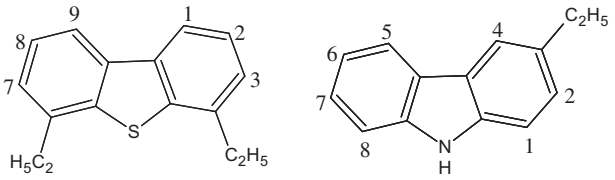

Fig. 2. Model compounds used in the present study: 4,6-diethyldibenzothiophene and 3-ethylcarbazole.

In practice, a viable ultra-deep HDS catalyst requires a high hydrogenation power and a high resilience to inhibition by nitrogen compounds [4,15,16]. Of the multitude of organonitrogen inhibitors, the most potent ones in ultra-deep HDS processes are alkylcarbazoles, which are abundantly present in severely hydrotreated oils [17–20]. Fig. 2 shows a pair of realistic model compounds for probing deep HDS chemistry and process, as will be discussed later. They are 4,6-diethyldibenzothiophene (46DEDBT) and 3-ethylcarbazole (3ECBZ); both of them rely primarily on catalyst's hydrogenation function to remove their heteroatoms [5,21]. A trace amount (five wppm as nitrogen atom) of 3ECBZ can drastically reduce the activity of a commercial $CoMo/Al_2O_3–SiO_2$ catalyst for desulfurizing 46DEDBT [21]. It is of both fundamental and practical importance to investigate 46DEDBT-3ECBZ competitive adsorption/reaction on various unsupported metal sulfides.

The present work is a kinetic characterization of unsupported ReS_2 prepared from $(NH_4)_4(Re_4S_{22})\cdot 2H_2O$ as deep HDS and HDN catalysts. We aim to gain a quantitative understanding of competitive adsorption dynamics using 46DEDBT and 3ECBZ as probe molecules. Through analyses and modeling of transient response data, the active site density and associated adsorption/reaction rate constants are determined. The results are compared with those for a commercial sulfided $CoMo/Al_2O_3–SiO_2$ catalyst in terms of intrinsic activity/selectivity and organonitrogen tolerance. The results shed some light on the nature of HDS–HDN interactions in ultra-deep HDS of petroleum fractions.

2. Experimental

2.1. Materials

The rhenium sulfide catalyst was prepared via a procedure different from those described in the review of Escalona et al. [12]. Specifically, it was prepared by the thermal decomposition of

$(NH_4)_4(Re_4S_{22})\cdot 2H_2O$ {rhenate(4-), tetra-μ_3-thioxohexakis[μ-(trithio)]tetra-, tetraammonium, dihydrate}, which was synthesized according to the procedure of Müller et al. [22]. The thus-synthesized solid product, after being pressed into pellets at 20,000 psig, was broken into granules and then heat treated in a tube furnace with a ramp rate 25 °C/min to 400 °C and held for one hour under a nitrogen flow at 200 cc/min. The resulting stoichiometry is approximately $ReS_{2.3}$. Upon exposure to the hydrogen atmosphere in the reactor, it loses excess sulfur, resulting in a stoichiometry of ReS_2 and a weight loss of about 4%. The ReS_2 catalyst, with a BET surface area of 55 m^2/g, was used in the form of 20–40 mesh granules in the transient response experiments. Both 46DEDBT and 3ECBZ were synthesized through known procedures.

2.2. Transmission electron microscope

Large agglomerates of ReS_2 particles were crushed into fines (~100 nm thick) using an agate mortar and pestle. The fines were dusted onto a standard, holey-carbon-coated, 200 mesh, Cu grid and transferred into a Philips CM200F TEM/(S)TEM. The microscope was operated in the bright field TEM imaging mode at an accelerating voltage of 200 kV. Randomly selected areas of the material were imaged at an "on screen" magnification of 175,000× using a Gatan model 694 CCD camera system and Gatan's Digital Micrograph v.2.5 software. Stack heights were measured from over 300 ReS_2 crystallites. Stack heights were plotted, and mean and median stack height values were calculated using KaleidaGraph v.3.0.

2.3. Reactors, procedures, and analyses

A cocurrent fixed-bed reactor, made of a 3/8-inch ID 316 stainless steel pipe, was operated isothermally in up-flow mode to avoid incomplete catalyst wetting and bypassing. Glass beads were charged in the fore and aft zones to achieve vapor–liquid equilibrium. To mitigate the axial dispersion effect, three grams catalyst was uniformly mixed with an equal volume of glass beads in the reactor central zone.

The liquid products were analyzed by GC/MS and GC using a 75% OV1/25% SW-10 fused silica capillary column. In addition, the total nitrogen was quantified by combustion and chemiluminescence using the Antek analyzer. Due to their low concentrations, individual HDN products were not measured. The carrier solvent dodecane (analytic pure grade) was essentially inert under the reaction conditions studied. The product gases were vented through a caustic scrubber followed by a wet test meter.

Table 1 lists the compositions of the feed mixtures (density = 0.72 g/cc), with the balance being dodecane.

Besides H_2S, the main products obtained from the HDS of 46DEDBT were identified to be diethylbiphenyls (C4BP), diethylcyclohexylbenzenes (C4CHB), ethylcyclohexylbenzenes (C2CHB), ethylbiphenyls (C2BP), ethylbenzenes, and ethylcyclohexanes. These products accounted for more than 98% of 46DEDBT converted. Diethylbicyclohexyl, ethylbicyclohexyl, biphenyl and cyclohexylbenzene were present in trace amounts. Products from partial hydrogenation of 46DEDBT, if present, are negligibly small in concentration.

Table 1
Feed compositions (wt.%).

Probe molecules	Feed A	Feed B
4,6-Diethyldibenzothiophene	0.8	0.8
3-Ethylcarbazole	0.0	0.112

2.4. Steady-state and transient experiments

The reaction conditions used in this study are 1.83 MPa hydrogen pressure, 265 °C, eight liquid weight hourly space velocity (WHSV), and 116 cc H_2/cc liquid feed. The sequence of the experiments is as follows. The reactor was started with feed A (1067 ppmw total sulfur as atoms) and pure hydrogen to obtain the baseline data in the absence of 3ECBZ (Steady State I). Following this, Feed A was replaced by Feed B (1067 ppmw sulfur plus 80 ppmw nitrogen as atoms) at time "zero" at the same conditions. After the reactor reached a new steady state (Steady State II), Feed A was put back on stream to strip the reversibly adsorbed nitrogen species off the catalyst, in an attempt to recover the lost HDS activity. To speed up the slow desorption of chemisorbed nitrogen species, the reactor temperature was raised to 300 °C for 5 h and then lowered back to 265 °C. The sulfur and nitrogen concentrations in the liquid effluents were intermittently measured throughout the entire experiment.

Since C4BP-to-C4CHB hydrogenation is very slow, the selectivity toward hydrogenation for an isothermal plug-flow reactor can be approximately gauged by the following concentration ratio in the liquid effluent

$$\gamma_{DEDBT} = \frac{\text{wt\% C4CHB in product}}{\text{wt\% C4BP in product}} \quad (1)$$

Note that γ_{DEDBT} in general is a decreasing function of temperature [21] and that the C2CHB/C2BP ratio roughly tracks the C4CHB/C2BP ratio.

3. Experimental results

3.1. TEM characterization

Fig. 3 is an electron micrograph of ReS_2. The bright field TEM image presents numerous ReS_2 crystallites. Each crystallite is composed of parallel "dark" and "light" layers. In the bright field TEM image, the "dark" layers correspond to rows of Re atoms, while the "light" layers correspond to rows of sulfur atoms. It is worthwhile noting that at this magnification, the double layer of sulfur atoms present between the layers of Re atoms is not resolved. It is also clear that these layered features are not immediately evident in all regions in the image. This effect arises from slight thickness changes across the field of view which affects focus. By watching the sample while slightly moving though either side of focus, it was possible to identify regions of the agglomerate where

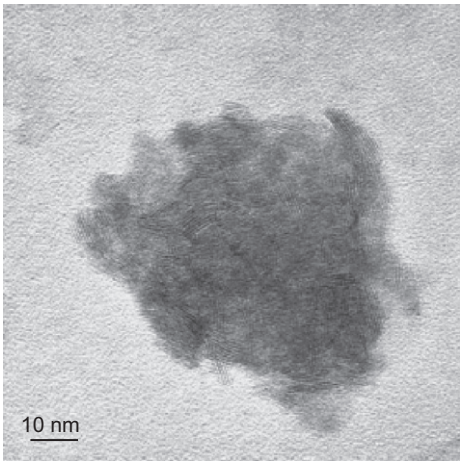

Fig. 3. Electron micrograph of ReS_2.

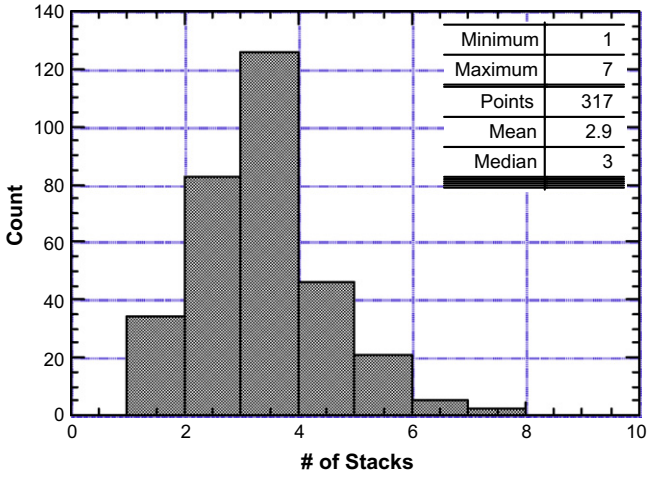

Fig. 4. Stack heights were measured from over 300 ReS_2 crystallites. Mean and median stack height values were calculated using KaleidaGraph v.3.0. The mean and median stack height values were about 2.9 and 3.0 layers per ReS_2 crystallite, respectively.

entire ReS_2 crystallites were visible. Their stack heights were measured from these regions, and the values are shown in Fig. 4. Crystallite stack heights ranging from 1 to 7 layers were observed in this analysis, and the mean and median stack height values were about 2.9 and 3.0 layers per ReS_2 crystallite, respectively.

3.2. HDS activity

Fig. 5 displays the transient response of DEDBT desulfurization on ReS_2 to a step jump in the feed nitrogen atom content from zero to 80 ppmw. Initially, at Steady State I (Feed A), the HDS level is about 96% at a WHSV of eight. During the breakthrough period, the HDS activity drops precipitately. When the system reaches Steady State II, sulfur removal decreases to about 17%. Evidently, the presence of 3ECBZ has a catastrophic effect on ReS_2's activity for desulfurizing 46DEDBT. As shown in Fig. 5, the catalyst was subsequently stripped of chemisorbed organonitrogen with Feed A at 265 °C to recover the HDS activity. After about 150 h of stripping, the reactor temperature was raised to 300 °C for five hours and then lowered back to 265 °C. As can be seen, after an initial rise in the HDS level, the recovery of the HDS activity becomes increasingly sluggish. The activity does not come close to its original level even after 200 h.

As mentioned, a similar transient response experiment was conducted with the sulfided $CoMo/Al_2O_3$–SiO_2 catalyst at 2.4 WHSV and otherwise identical conditions [21]. The HDS level dropped from 70% at Steady State I to less than 10% at Steady State II. In terms of intrinsic gravimetric activity (pseudo-first-order rate constant, cc liquid feed/g cat/s), ReS_2 shows approximately a 9-fold activity advantage over sulfided $CoMo/Al_2O_3$ at Steady State I. By intrinsic, it is meant that the HDS activity is measured in the absence of any inhibitor such as nitrogen or aromatic species.

3.3. Hydrogenation selectivity

Fig. 6 shows the behavior of γ_{DEDBT} during the breakthrough and stripping periods. Initially, γ_{DEDBT} is about 11, indicating an overwhelming preference for the hydrogenation pathway. For perspective, $\gamma_{DEDBT} \sim 5$ for the $CoMo/Al_2O_3$–SiO_2 catalyst at the same conditions [21]. Referring to Fig. 6, γ_{DEDBT} drops rapidly from ~11 to as low as ~0.3 after the 3ECBZ assault. That is, the inhibiting process is so selective toward the hydrogenation sites that the hydrogenation pathway is almost completely shut off for HDS at Steady State II. And the chemisorption of 3ECBZ is so strong that the adsorbed nitrogen species would not come off the catalyst surface easily. As a result, a complete recovery of the hydrogenation function does not seem possible. This quasi-irreversible behavior is not uncommon [23–25]. The long-lingering adsorbed nitrogen species tend to polymerize and eventually form coke [26].

4. Modeling of inhibition dynamics

4.1. Simplifying assumptions

Before setting out the model equations, we make the following simplifying assumptions. (1) The catalyst surface is Langmuirian and energetically uniform; (2) Hydrogen is adsorbed on sites that are different from those for the adsorption of sulfur and nitrogen species; (3) For adsorption of organosulfur and organonitrogen species, only the hydrogenation sites are considered due to overwhelming dominance of the hydrogenation pathway; (4) Because of the high hydrogen/46DEDBT volume ratio, the hydrogen

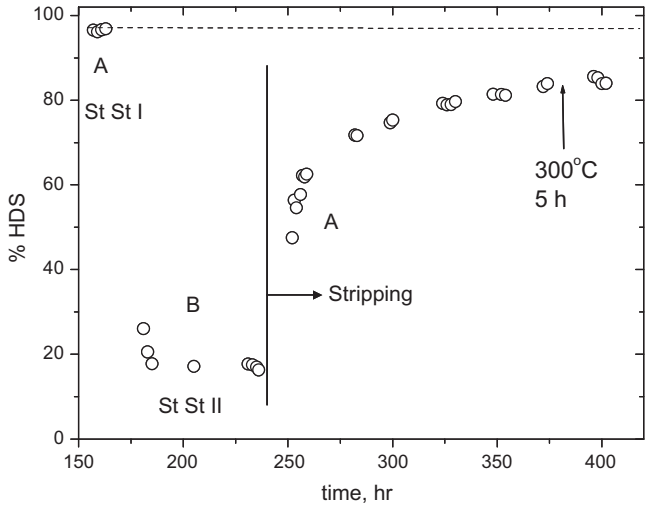

Fig. 5. Percentage of HDS vs. time (h) obtained with ReS_2; Feed A was used at Steady State I, Feed B was used in Steady State II; 265 °C, 8 WHSV, 1.83 MPa, and 116 cc H_2/cc liquid feed; Feed A was used for stripping; After the 370th hour, the stripping temperature was raised to 300 °C for 5 h.

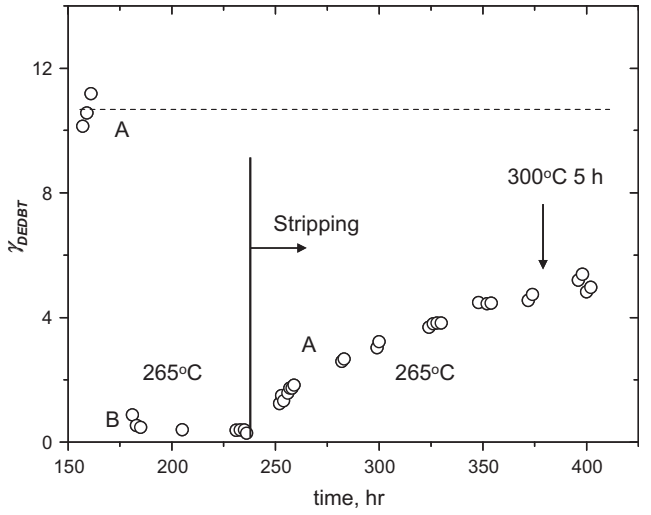

Fig. 6. γ_{DEDBT} vs. time (h) obtained with ReS_2; Feed A was used at Steady State I, Feed B was used in Steady State II; 265 °C, 8 WHSV, 1.83 MPa, and 116 cc H_2/cc liquid feed; Feed A was used for stripping; After the 370th hour, the stripping temperature was raised to 300 °C for 5 h.

pressure is constant and the surface hydrogen coverage is high; (5) The effect of molar change due to reaction is negligible; (6) The inhibiting effects of H_2S, NH_3, and heteroatom-free hydrocarbons are relatively insignificant compared with that of organonitrogen species; (7) Axial dispersion effect and the velocity changes due to adsorption are negligible; (8) The concentrations of sulfur and nitrogen compounds are constant throughout the catalyst particles; (9) The reactor is isothermal and isobaric, with negligible mass transfer effects; (10) Both HDS and HDN occur irreversibly on the catalyst surface and hydrogen addition is not rate limiting; (11) Catalyst deactivation by coking is negligible on the time scale of the inhibition event; and (12) Liquid feed and hydrogen reach physical equilibrium before entering the catalyst bed.

Let S and N be the sulfur atom and nitrogen atom concentrations in the flowing stream (micromole/cc feed), respectively. Here, both S and N include sulfur- and nitrogen-containing heterocyclic species formed from conversions of 46DEDBT and 3ECBZ. Also, let q_n and q_s be the adsorbed nitrogen and sulfur atom concentrations, respectively. Denoting q_m as the catalyst's total chemisorption capacity on the hydrogenation sites, then $\theta_n = q_n/q_m$ is the fractional coverage of adsorbed nitrogen. For sulfur species, k_s, k_s', and k_{HDS} are the adsorption rate constant (cc liquid/s/μmole), desorption rate constant (s^{-1}), and surface HDS rate constant (s^{-1}), respectively. The corresponding rate constants for nitrogen species are k_n, k_n', and k_{HDN}.

To construct a model that is as simple as possible necessitates further pruning. To this end, the slow desorption of organonitrogen species can be considered as frozen on the time scale of the inhibition transient. At the other extreme, the surface HDS is too fast to influence the sluggish inhibition process ($k_{HDS} \gg k_{HDN}$ because the C–S bond is much weaker than the C–N bond). The desorptions of nitrogen or sulfur compounds are not fast enough to attain a local adsorption–desorption equilibrium as the nitrogen and sulfur adsorption fronts travel down the bed during the breakthrough period. The consequence is that the inhibition transient is mainly governed by the interplay of sulfur adsorption, nitrogen adsorption, and surface HDN.

In light of the above, we set $k_nN_f \gg k_n'$, $k_{HDN} \gg k_n'$, $k_n \gg k_s$, $k_{sa}S_f \ll k_{HDS}$, and $q_s \ll q_n$. These stipulations were justified previously [16,27,28]. It should be noted that here we essentially use organonitrogen adsorbates to "sample" (or "titrate") the active sites in situ. Thus, q_m is a measure of the maximum site density with the units of μmole nitrogen adatom/g catalyst.

Reactor specifications are bed void fraction, $\varepsilon = 0.3$; catalyst particle density, $\rho_p = 1.15$ g/cc; and bed length, $L = 3.82$ cm. The concentrations of sulfur and nitrogen atoms in the feed are $S_f = 58.8$ μmole/cc and $N_f = 4.1$ μmole/cc, respectively. With v being the superficial fluid velocity based on empty reactor, the transient response of the system after introducing 3ECBZ (time $t > 0$) is described by the following plug-flow, one-dimensional model [27]

(i) S mass balance in the fluid phase

$$v\frac{\partial S}{\partial z} + \varepsilon\frac{\partial S}{\partial t} + (1-\varepsilon)\rho_p k_s S(q_m - q_n) = 0 \tag{2}$$

(ii) N mass balance in the fluid phase

$$v\frac{\partial N}{\partial z} + \varepsilon\frac{\partial N}{\partial t} + (1-\varepsilon)\rho_p k_n N(q_m - q_n) = 0 \tag{3}$$

(iii) N mass balance in the solid phase

$$\frac{\partial q_n}{\partial t} = k_n N(q_m - q_n) - k_{HDN} q_n \tag{4}$$

The model has four parameters (k_{HDN}, k_n, k_s, and q_m). Only one of the four parameters is adjustable due to steady-state constraints [27]. The required boundary conditions at $z = 0$ ($t > 0$) are $S = S_f$ and $N = N_f$. The initial conditions correspond to Steady State I. Thus, at $t = 0$ ($z \geqslant 0$), we have $N = q_n = 0$ and

$$v\frac{dS}{dz} = -(1-\varepsilon)\rho_p k_s q_m S \tag{5}$$

where $S = S(z)$ at $t = 0$. Eq. (5) can be readily integrated with the reactor inlet condition $S(0) = S_f$ to yield

$$S(z) = S_f \exp\left[-\frac{(1-\varepsilon)\rho_p k_s q_m}{v} z\right] \tag{6}$$

With the above boundary and initial conditions, Eqs. (2)–(4) were solved numerically by using an implicit finite difference scheme. The parameter estimation was carried out through optimization with constraints derived from steady-state experiments. The details can be found in an earlier paper [27].

In practice, what matter are the HDS and HDN behaviors at Steady State II, which are dictated by the following equations:

$$v\frac{dS}{dz} = -\frac{(1-\varepsilon)\rho_p k_s q_m}{(1 + k_n N/k_{HDN})} S \tag{7}$$

$$v\frac{dN}{dz} = -\frac{(1-\varepsilon)\rho_p k_n q_m}{(1 + k_n N/k_{HDN})} N \tag{8}$$

Thus, HDS is inhibited by nitrogen species, whereas HDN is self-inhibited. Recall that a basic tenet of the present treatment is that the inhibiting effect of sulfur species is negligibly small compared with that of nitrogen species. And the desorption of nitrogen species is too slow ($k_n' \ll k_{HDN}$) to be kinetically relevant. Hence, the extent of organonitrogen inhibition is driven by k_{HDN}, which governs surface concentration of chemisorbed nitrogen species.

4.2. Governing parameters and steady-state behavior

To identify governing parameters, Eqs. (7) and (8) are made dimensionless with the following scaled variables: $s = S/S_f$, $n = N/N_f$, and $\xi = z/L$, Also, the space time τ is defined as $\tau = (1-\varepsilon)\rho_p L/v$. Eqs. (7) and (8) become

$$\frac{ds}{d\xi} = -\frac{k_s q_m \tau}{1 + gn} s \tag{9}$$

$$\frac{dn}{d\xi} = -\frac{k_n q_m \tau}{1 + gn} n \tag{10}$$

Here, s is slaved to nitrogen concentration; s cannot be determined unless n is obtained from solving Eq. (10). The corresponding boundary conditions are $s = n = 1$ at $\xi = 0$. The dimensionless parameter g in the denominator is defined as

$$g \equiv \frac{k_n N_f}{k_{HDN}} \tag{11}$$

Thus, g represents the ratio of the nitrogen adsorption rate to the surface HDN rate. It is a measure of the inhibition intensity. It is relevant to point out that if the desorption is fast enough to maintain a local adsorption–desorption equilibrium ($k_n' \gg k_{HDN}$), then the inhibition intensity should be gauged by $\bar{g} \equiv k_n N_f/k_n' = KN_f$ where $K \equiv k_n/k_n'$ is the adsorption equilibrium constant.

Dividing Eq. (9) by Eq. (10), we obtain

$$\frac{ds}{dn} = p\frac{s}{n} \tag{12}$$

At a given set of temperature, pressure, and hydrogen treat gas rate, s and n are functions of the space time τ. The dimensionless parameter p is defined by

$$p \equiv \frac{k_s}{k_n} \tag{13}$$

Hence, p is an adsorption ratio reflecting the catalyst's adsorption affinity for sulfur species relative to that for nitrogen species.

It transpires from the above development that the inhibition dynamics is characterized by g and p, both of which are functions of catalyst properties for a given feed. Eq. (12) upon integration from $\xi = 0$ to $\xi = 1$ (reactor outlet) yields a relationship between s and n at the reactor outlet at Steady State II

$$s(\tau) = n(\tau)^p \tag{14}$$

The simple model-compound model represented by Eqs. (9) and (10) captures two characteristic features of real-feed ultra-deep HDS: sulfur removal is predominantly controlled by nitrogen species [15] and nitrogen removal is largely governed by self-inhibition [20].

5. Results and discussions

5.1. Rate parameters and active site densities

The model parameters obtained from data fitting are listed in Table 2, which also includes the results obtained previously for the sulfided $CoMo/Al_2O_3–SiO_2$ catalyst [27].

The solid curves in Fig. 7 are model predictions, which compare well with the measured nitrogen exit concentration (wppm) and the percentage of HDS as functions of elapsed hour after introducing the 3ECBZ-containing feed. As can be seen, the dynamic process leading up to Steady State II is well predicted by the model.

Table 2
Model parameters for unsupported ReS_2 and $CoMo/Al_2O_3–SiO_2$.

Parameters	Unsupported ReS_2	$CoMo/Al_2O_3–SiO_2$
k_s, cc feed/s/μmole	154×10^{-6}	6.7×10^{-6}
k_n, cc feed/s/μmole	78.9×10^{-5}	2.7×10^{-5}
k_{HDN}, s^{-1}	121×10^{-6}	6.3×10^{-6}
q_m, μmole N adatom/g cat	96.4	271.4
p	0.2	0.25
g	27	17

(265 °C, 1.83 MPa hydrogen pressure)

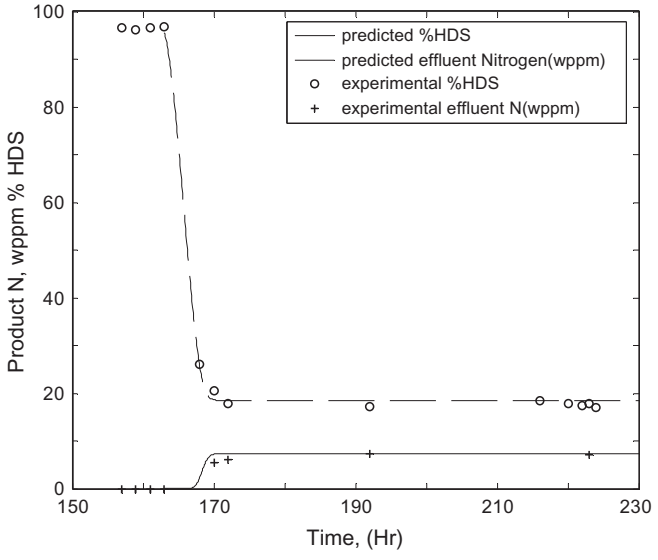

Fig. 7. Percentage of HDS and total nitrogen concentration (wppm) at reactor exit as functions of elapsed time following introduction of 3-ethylcarbazole; ReS_2; 265 °C, 8 WHSV, 1.83 MPa, and 116 cc H_2/cc liquid feed. Solid curves are predicted from the model.

5.2. Spatiotemporal behavior

Having determined the model parameters, we now examine the spatiotemporal behavior of the system. Fig. 8 shows the sulfur concentration in the fluid phase as a function of bed position at successive elapsed times. Initially ($t = 0$ h), the reactor sulfur profile in the absence of 3ECBZ shows an exponential decline. Subsequently, the fluid sulfur content increases as the concentration wave travels toward the reactor outlet. The advancing sulfur front is not at a local adsorption–desorption quasi-equilibrium with the active sites. After 10 h of nitrogen assault, the majority of the active sites in the bed are occupied by nitrogen species; the bulk of 46DEDBT stays in the fluid phase as a "spectator." As a result, the sulfur profile remains nearly flat and becomes only slightly concave downward near the reactor outlet where some active sites have not yet been blocked at that moment. The sulfur concentration in reactor effluent increases as time goes by. The speed with which the sulfur travels through the bed is faster than that calculated for the $CoMo/Al_2O_3–SiO_2$ catalyst.

Fig. 9 shows multiple snapshots of nitrogen concentration in the fluid phase resulting from the combined action of adsorption and surface HDN reaction. The moving front is accompanied by a decreasing N due to HDN whose rate plays a pivotal role in the inhibition process. The model must account for surface HDN reaction; otherwise, it would not predict the nitrogen breakthrough curve and the steady-state nitrogen concentration. During the breakthrough period, the catalyst bed is divided into two zones. The upstream zone is saturated with organonitrogen and performing HDN, while the downstream zone has not seen organonitrogen yet and is carrying out HDS.

Fig. 10 shows the percent coverage of active sites ($100q_n/q_m$) by nitrogen species as a function of bed length at different elapsed times. Prior to the breakthrough, the catalyst bed near the reactor outlet is virtually free of nitrogen species as the upstream bed adsorbs and denitrogenates all incoming nitrogen species. After 10 h, the majority of active sites are occupied by nitrogen species, thus diminishing HDS almost completely.

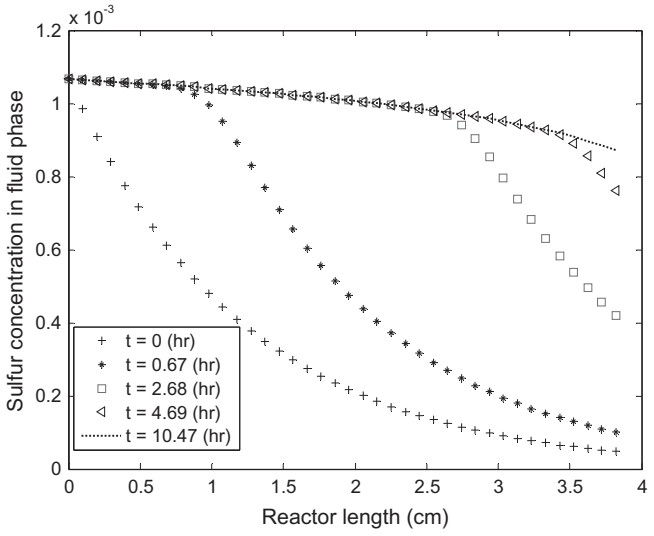

Fig. 8. Predicted moving sulfur concentration front $s = S/S_f$ for different elapsed times. ReS_2 catalyst.

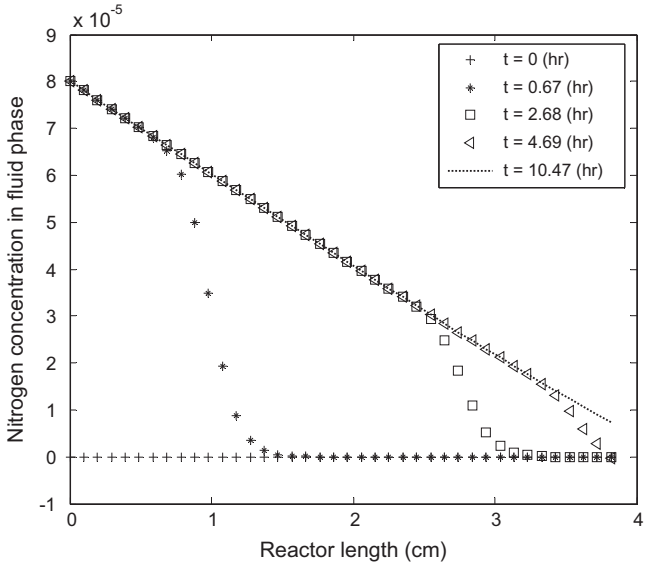

Fig. 9. Predicted moving nitrogen concentration front $n = N/N_f$ for different elapsed times. ReS_2 catalyst.

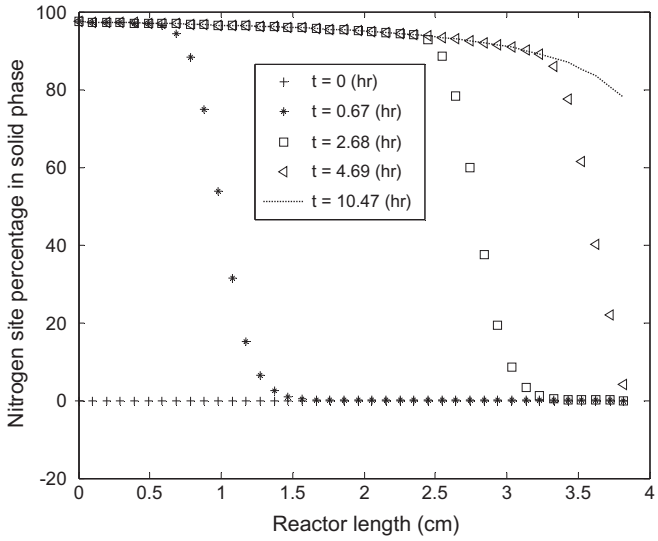

Fig. 10. Percent site coverage by adsorbed nitrogen, $100q_n/q_m$, for different elapsed times. ReS_2 catalyst.

5.3. ReS_2 vs. sulfided $CoMo/Al_2O_3–SiO_2$

For perspective, here we begin by a recapitulation of the results on the sulfided $CoMo/Al_2O_3–SiO_2$ catalyst [27]. Referring to Table 2, the catalyst adsorbs 3ECBZ about 17 times faster ($g = 17$) than it denitrogenates. It is highly selective toward the adsorption of 3ECBZ. As a result, the surface is swarmed with adsorbed nitrogen species. Table 2 also indicates that k_s and k_n for unsupported ReS_2 are much higher than those for $CoMo/Al_2O_3–SiO_2$. ReS_2's k_{HDN} is higher than that of $CoMo/Al_2O_3–SiO_2$ by a factor of about 19. Moreover, the density of active site q_m on ReS_2 is about one-third that on $CoMo/Al_2O_3–SiO_2$. This implies that the HDN surface turnover frequency on ReS_2 is much higher than that on $CoMo/Al_2O_3–SiO_2$.

Relative to sulfided $CoMo/Al_2O_3–SiO_2$, ReS_2 has a higher selectivity for 3ECBZ adsorption as can be seen from the p values listed in Table 2. As an interesting aside, this result bears some resemblance to the binding powers of 46DEDBT and 3ECBZ on a Ru organometallic complex [29]. The latter serves as a model for π-adsorption through six carbon atoms to a metal site on a catalyst surface. Specifically, it was found that the relative binding powers of 3ECBZ and 46DEDBT in $CpRu(\eta^6\text{-arene})^+$ complexes are 6.5 and 1.1, respectively. So the binding (adsorption) ratio is $1.1/6.5 = p = 0.17$, which is comparable to $p = 0.2$ for ReS_2. Rhenium sulfide and ruthenium sulfide have similar metal–sulfur bond energies [3]. Based on these observations, it appears that the relative binding (adsorption) tendencies of 46DEDBT and 3ECBZ on Re and Ru are comparable.

To compare the relative susceptibility of HDS to organonitrogen inhibition between ReS_2 and sulfided $CoMo/Al_2O_3–SiO_2$, we compare the g values for the two catalysts. The ReS_2 catalyst gives $g = 27$ vs. $g = 17$ for $CoMo/Al_2O_3–SiO_2$. This indicates that although ReS_2 is intrinsically more active than $CoMo/Al_2O_3–SiO_2$ for desulfurizing 46DEDBT, it is more vulnerable to 3ECBZ inhibition. As a result, ReS_2 suffers a greater loss of HDS activity than $CoMo/Al_2O_3–SiO_2$ in the presence of 3ECBZ. This is consistent with ReS_2's high hydrogenation power (high γ_{DEDBT}). A quantitative analysis of the relative nitrogen tolerance of hydrogenation and hydrogenolysis sites has been made for the sulfided $CoMo/Al_2O_3–SiO_2$ catalyst [16].

Fig. 11 shows $s(\tau)$ and $n(\tau)$ as functions of τ for the ReS_2 catalyst. The dashed line represents the HDS of 46DEDBT in the absence of 3ECBZ. In the presence of 3ECBZ, sulfur removal (solid curve) is severely inhibited by nitrogen species. The self-inhibiting effect of nitrogen species is also evident. When both 46DEDBT and 3ECBZ are present, the selectivity of ReS_2 for HDN is far higher than that for HDS.

5.4. Interactions between HDS and HDN

This section aims to connect the 46DEDBT-3ECBZ model system with deep HDS in the real world. Let us consider a hypothetical middle distillate containing 1 wt.% sulfur (taking a round number). Meeting the 10 wppm product sulfur specification means an ultra-deep HDS level higher than 99.9% ($s = 0.001$). Even for low-sulfur (e.g., prehydrotreated) feedstocks, a reduction of from, say, 500 wppm feed sulfur to 10 wppm product sulfur means a deep HDS level as high as 98% ($s = 0.02$). Polynuclear aromatics, due to their heaviness/size [30] and high concentration, are generally the dominant inhibitor when the HDS level is not deep (say, product sulfur level >500 wppm). As the desulfurization gets deeper,

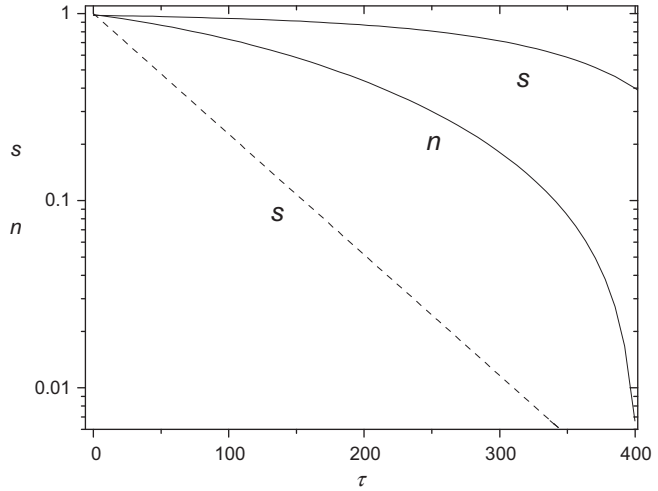

Fig. 11. Semi-logarithmic plots of calculated s and n vs. space time τ for unsupported ReS_2. The dashed line s is for the HDS of 46DEDBT in the absence of 3ECBZ.

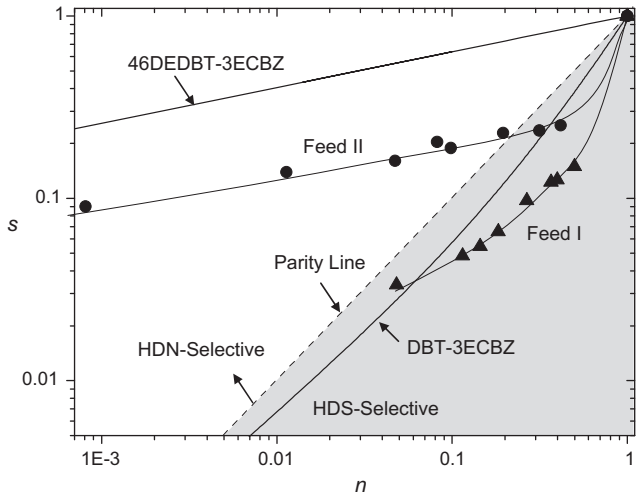

Fig. 12. ln(s) vs. ln(n) data on two different catalysts for two different petroleum fractions, Feedstocks I and II [5]. The two solid straight lines are calculated from model-compound data obtained with 46DEDBT-3ECBZ and DBT-3ECBZ probes. The dashed line represents equal selectivity for HDN and HDS.

residual nitrogen heterocycles emerge as the dominant inhibitor [15], as alluded to earlier. In many practical situations, the objective of achieving less than 10 wppm product sulfur cannot be met unless the product nitrogen level is reduced to a sufficiently low level. Thus, here one deals with a process that requires super-high conversions for both HDS and HDN. This situation can be succinctly described by the ln(s) vs. ln(n) plot over multiple decades, as illustrated in Fig. 12. This figure shows how the HDS trajectory becomes increasingly influenced by nitrogen inhibition as the reaction (or space) time increases. Here, the experimental data on real feeds (Feedstocks I and II) are taken from Fig. 16 in Ref. [5]. If a catalyst happens to be equally selective toward HDS and HDN, then its heteroatom removal trajectory follows the dashed line with $p = 1$ (parity line). Above the parity line is the HDN-selective region. Typically, the trajectory starts in the HDS-selective region (shaded area), in which reactive sulfur species are desulfurized. As the HDS level gets deeper, the trajectory becomes more and more curved toward the HDN-selective region due to increasingly strong organonitrogen inhibition to the HDS of hindered DBTs. Here, partially hydrogenated nitrogen heterocycles can be more inhibiting than their parent molecules [20]. For difficult-to-desulfurize feedstocks (e.g., catalytic light cycle oil that contains high levels of alkylcarbazoles), a sufficiently deep HDS may not be achievable within the operating constraints of a commercial HDS reactor. An example is Feedstock II shown in Fig. 12. This feedstock has a lower API gravity than Feedstock I. Both feeds have approximately the same level of total nitrogen, 705 wppm for Feed I and 740 ppm for Feed II. However, the nitrogen heterocycles in Feed I were found to be dominated by six-membered species such as quinolines, whereas those in Feed II are predominantly five-membered species such as carbazoles [5].

Now return to the model-compound experiments using the 46DEDBT-3ECBZ probe on unsupported ReS_2. Eq. (14) can be rewritten as

$$\ln[s(\tau)] = p \ln[n(\tau)] \tag{15}$$

Thus, for the model-compound system, $s(\tau)$ and $n(\tau)$ are linearly related to each other on a double logarithmic plot of ln(s) vs. ln(n), with a slope of p. As Fig. 12 shows, the ln(s) vs. ln(n) plot is a rather flat straight line due to the small p value of 0.2. Although not shown, the same plot for the $CoMo/Al_2O_3$–SiO_2 catalyst is also rather flat because of a small p of 0.25. With either catalyst, the slope is comparable to that of the trajectory for Feedstock II at high HDS levels (>80% or $s < 0.2$). This confirms that 46DEDBT and 3ECBZ are realistic model compounds for probing HDS–HDN interactions in the ultra-deep HDS of difficult-to-desulfurize middle distillates. For perspective, Fig. 12 also shows the ln(s) vs. ln(n) plot for the DBT-3ECBZ probe over the $CoMo/Al_2O_3$–SiO_2 catalyst. The slope is steep because 3ECBZ is much less inhibiting to the HDS of DBT [21].

Table 3
Equivalent pseudo-first-order gravimetric rate constants for HDN of 3ECBZ.

	ReS_2	$CoMo/Al_2O_3$
$k_o \times 10^3$	2.85	0.42

Units: cc liquid feed/g cat/s.

5.5. HDN activities

In practice, it is the performance of the catalyst at Steady State II that matters. Fig. 7 shows that ReS_2 gives rise to an effluent liquid containing about 7 wppm nitrogen at Steady State II. This corresponds to a remarkably high HDN of 91% at a WHSV of eight, notwithstanding a strong self-inhibition effect. By contrast, the $CoMo/Al_2O_3$–SiO_2 catalyst gives a 58% HDN at a low WHSV of 2.4 [21,27]. The corresponding 46DEDBT HDS levels for ReS_2 and $CoMo/Al_2O_3$–SiO_2 are ~17% and ~10%, respectively. These results indicate that ReS_2 essentially behaves as a deep HDN catalyst. In what follows we compare the HDN activities of unsupported ReS_2 and sulfided $CoMo/Al_2O_3$–SiO_2 based on results shown in Table 2.

Integrating Eq. (10) from $\xi = 0$ to $\xi = 1$ gives n at the reactor outlet

$$g[1 - n(\tau)] - \ln n(\tau) = k_n q_m \tau \tag{16}$$

Since $g \gg 1$ for both catalysts, the first term on the left-hand side dominates the HDN behavior over a wide range of HDN levels. Eq. (16) can then be approximately written as

$$n(\tau) \approx 1 - \left(\frac{k_n q_m}{g}\right)\tau = 1 - k_o \tau \tag{17}$$

Thus, k_o is viewed as an approximate overall HDN rate constant defined as

$$k_o \equiv \frac{k_n q_m}{g} = \frac{k_{HDN} q_m}{N_f} \tag{18}$$

Here, k_o can also be regarded as an equivalent pseudo-first-order gravimetric rate constant. The concept of equivalent first-order rate constant was discussed in Ref. [5]. Note that k_o is inversely proportional to the feed nitrogen concentration N_f, which has a direct bearing on real-feed HDN [20].

Based on the parameter listed in Table 2, the k_o values for unsupported ReS_2 and sulfided $CoMo/Al_2O_3$–SiO_2 can be calculated and are listed in Table 3.

Since we neglect the second term on the left-hand side of Eq. (16), the activity advantage of the unsupported ReS_2 catalyst shown in Table 3 is somewhat conservative. What we can say is that ReS_2 gives about a sevenfold HDN activity advantage over the sulfided $CoMo/Al_2O_3$–SiO_2 catalyst.

6. Concluding remarks

Using 46DEDBT and 3ECBZ as model compounds provides useful information on the HDS–HDN interactions in the deep HDS of petroleum middle distillates. The unsupported ReS_2 catalyst prepared from $(NH_4)_4(Re_4S_{22})\cdot 2H_2O$ has an unusually strong

hydrogenation function. As a result, it gives about a 9-fold activity advantage over a commercial sulfided $CoMo/Al_2O_3–SiO_2$ catalyst for desulfurization of 46DEDBT in the absence of 3ECBZ. But it suffers a disproportionately greater loss of HDS activity than $CoMo/Al_2O_3–SiO_2$ in the presence of 3ECBZ. In other words, ReS_2 is less resilient to 3ECBZ inhibition than $CoMo/Al_2O_3–SiO_2$. The latter has a higher selectivity for hydrogenolysis (lower γ_{DEDBT}). A recent study has shown that hydrogenolysis sites are more capable of mitigating the impact of organonitrogen inhibition than hydrogenation sites [16].

The unsupported ReS_2 catalyst shows about a sevenfold HDN activity advantage over the sulfided $CoMo/Al_2O_3–SiO_2$ catalyst. It is also much more selective for HDN in simultaneous HDS and HDN experiments. This can be attributed to a high adsorption affinity for organonitrogen species coupled with a fast C–N bond cleavage rate. The high HDN activity results from a greater intrinsic activity per active site, rather than a higher site density. The nature of the active sites on ReS_2 and on $CoMo/Al_2O_3–SiO_2$ should be very different, even though ReS_2 and MoS_2 are structurally similar in certain respects. It is of great interest to know whether metallic brim sites exist on ReS_2.

A highly hydrogenative ReS_2 should be regarded as a catalyst primarily for deep HDN. It is relevant to point out that the nitrogen content of refinery hydroprocessing feedstocks has been increasing over the years. The objectives of two key refinery conversion processes, fluid catalytic cracking and hydrocracking, cannot be achieved unless the feed nitrogen level is reduced to a sufficiently low level. Developments of new or improved HDN catalysts and processes have been and will continue to be important in the years ahead [31].

As for ultra-deep HDS applications, ReS_2 should be used with a hydrogenolysis-selective catalyst in a properly configured stacked bed to give an activity synergism. This catalyst-stacking strategy has been demonstrated with a highly hydrogenative $Ni_{0.5}Mn_{0.5}Mo$ sulfide catalyst [4]. Also, the low nitrogen tolerance of the ReS_2 catalyst may be improved through incorporation of promoter metals such as cobalt and/or nickel. Co- or Ni-promoted Re sulfide catalysts, in unsupported or supported form, are more HDS-selective than their unpromoted counterparts, suggesting that they may be more hydrogenolysis selective [32,33].

Acknowledgment

Q. Shen from the Department of Chemical Engineering at the University of Texas at Austin acknowledges a summer internship supported by ExxonMobil Research and Engineering Company.

References

[1] H. Topsøe, B.S. Clausen, F.E. Massoth, Hydrotreating Catalysis, Springer-Verlag, 1996.
[2] B.C. Gates, H. Topsøe, Polyhedron 16 (1997) 3213.
[3] N. Hermann, M. Brorson, H. Topsøe, Catal. Lett. 65 (2000) 169.
[4] T.C. Ho, Catal. Today 98 (2004) 3.
[5] T.C. Ho, Catal. Today 130 (2008) 206.
[6] T.C. Ho, Catal. Lett. 89 (2003) 21.
[7] S. Eijsbouts, S.W. Mayo, K. Fujita, Appl. Catal. A: Gen. 322 (2007) 58.
[8] J.V. Lauritsen, M. Nyberg, J.K. Nørskov, B.S. Clausen, H. Topsøe, E. Lægsgaard, F. Besenbacher, J. Catal. 224 (2004) 94.
[9] V. Petkov, J.L. Billinge, P. Larson, S.D. Mahanti, T. Vogt, K.K. Rangan, M.G. Kanatzidis, Phys. Rev. B 65 (2002) 092105.
[10] H.H. Murray, S.P. Kelty, R.R. Chianelli, C.S. Day, Inorg. Chem. 33 (1994) 4418.
[11] H.J. Lamfers, A. Meetsma, G.A. Wiegers, J.L. de Boer, J. Alloys Compd. 241 (1996) 34.
[12] N. Escalona, M. Vrinat, D. Laurenti, F.J. Gil Llambias, Appl. Catal. A: Gen. 322 (2007) 113.
[13] C.J.H. Jacobsen, E. TÖrnqvist, H. Topsøe, Catal. Lett. 63 (1999) 179.
[14] M. Breysse, E. Furimsky, S. Kasztelan, M. Lacroix, G. Perot, Catal. Rev. 44 (2002) 651.
[15] T.C. Ho, G.E. Markley, Appl. Catal. A: Gen. 267 (2004) 245.
[16] T.C. Ho, Q. Liang, J. Catal. 269 (2010) 291.
[17] I. Ignatiadis, M. Kuroki, P.J. Arpino, J. Chromatogr. 366 (1986) 251.
[18] S.D. Sumbogo Murti, H. Yang, K.H. Choi, Y. Korai, I. Mochida, Appl. Catal. A: Gen. 252 (2003) 331.
[19] W. Kanda, I. Siu, J. Adjaye, A.E. Nelson, M.R. Gray, Energy Fuels 18 (2004) 539.
[20] T.C. Ho, Appl. Catal. A: Gen. 378 (2010) 52.
[21] T.C. Ho, J. Catal. 219 (2003) 442.
[22] A. Müller, E. Krickemeyer, H. Bögge, Z. Anorg. Allg. Chem. 554 (1987) 61.
[23] E. Furimsky, F.E. Massoth, Catal. Today 52 (1999) 381.
[24] T.C. Ho, J. Sobel, Catal. Lett. 99 (2005) 109.
[25] P. Steiner, E.A. Blekkan, Fuel Proc. Technol. 79 (2002) 1.
[26] E. Furimsky, F.E. Massoth, Catal. Rev. 47 (2005) 297.
[27] T.C. Ho, D. Nguyen, J. Catal. 222 (2004) 450.
[28] T.C. Ho, D. Nguyen, Chem. Eng. Commun. 193 (2006) 460.
[29] M.G. Choi, T.C. Ho, R.J. Angelici, Organometallics 27 (2008) 1098.
[30] S. Korre, M. Neurock, M.T. Klein, R.J. Quann, Chem. Eng. Sci. 49 (1994) 4191.
[31] E. Furimsky, F.E. Massoth, Catal. Rev. Sci. Eng. 47 (2005) 297–489.
[32] N. Escalona, J. Ojeda, P. Baeza, R. Garcia, J.M. Palacios, J.L.G. Fierro, A. Lopez Agudo, F.J. Gil-Liambias, Appl. Catal. A: Gen. 287 (2005) 47.
[33] J. Ojeda, N. Escalona, J.M. Palacios, M. Yates, J.L.G. Fierro, A. Lopez Agudo, F.J. Gil-Liambias, Appl. Catal. A: Gen. 350 (2008) 6.